Magnetic 4*d* monoatomic rows on Ag vicinal surfaces

V. Bellini, N. Papanikolaou, R. Zeller, and P. H. Dederichs
Institut für Festkörperforschung, Forschungszentrum Jülich, D-52425 Jülich, Germany
(Received 25 October 2000; revised manuscript received 25 April 2001; published 31 July 2001)

The magnetic properties of 4*d* monoatomic rows on Ag substrates have been studied by *ab initio* calculations using the screened Korringa-Kohn-Rostoker (SKKR) Green's function method within density functional theory (DFT) in its local spin density approximation (LSDA). The rows were placed at step-edge (step decoration) and on terrace positions of different vicinal Ag surfaces, i.e., fcc (711), fcc (410), and fcc (221). The results for the magnetic moments are explained in terms of the different coordination numbers of the row atoms and the different hybridization between the rather extended 4*d* orbitals of the row atoms and the *sp*-like valence electrons of the Ag substrates. For the fcc (711) vicinal surface, we explore the possibility of antiferromagnetic coupling between the atoms in each row and discuss, by means of total energy calculations, the stability of the antiferromagnetic solutions with respect to the ferromagnetic ones.

DOI: 10.1103/PhysRevB.64.094403 PACS number(s): 75.75.+a, 75.70.Ak, 75.70.Rf

I. INTRODUCTION

In the last decades many efforts have been devoted to the understanding of the influence of spatial confinement on the magnetic properties of ultrathin transition metal films.[1] Among all materials, the ones which are on the borderline of magnetism are particularly interesting to study, since they exhibit large and more unexpected changes in their magnetic properties. The 4*d* and 5*d* elements are perhaps the best candidates for such studies; nonmagnetic as bulk metals, some of these elements were predicted to be magnetic as two-dimensional monolayers, e.g., Tc, Ru, Rh, Os, and Ir overlayers on the Ag(001) or Au(001) surfaces.[2–4] On the extreme side of spatial confinement, i.e., as adatoms on surfaces, they indeed were predicted on the Ag, Cu, Pd, and Pt substrates to show large magnetic moments,[5,6] which are of the same order of magnitude as the ones observed for 3*d* impurities[7] in the bulk.

While in the past many experimental methods have been used to observe ferromagnetism of monolayers, rather few of them have the necessary sensitivity to detect the magnetic moments of ''surface impurities.'' Motivated by the unexpected theoretical findings presented by Lang *et al.*,[5] Bergmann and co-workers performed several measurements for adatoms and clusters up to the monolayer regime of 4*d* elements on Ag and Au substrates by means of the weak localization method.[8–10] They succeeded to confirm existence of local magnetic moments and detected a magnetic moment for Nb impurities on Ag and Mo impurities on Au, in agreement with the above calculations, whereas no magnetism was observed for the 4*d* monolayers.

If, as discussed briefly above, zero-dimensional (impurities) and two-dimensional (monolayers) 4*d* structures on noble metals have received considerable attention, very few studies so far have been presented for one-dimensional systems, i.e., monoatomic rows. On the theoretical side, due to the large computational effort needed to balance the reduction of symmetry, this problem has only been tackled by semiempirical methods rather than by *ab initio* approaches. By means of tight-binding model Hamiltonians the magnetic anisotropy energy (MAE) of finite-length chains of 3*d* elements[11] and row-row magnetic interactions for Co rows on Pd(110) (Ref. 12) have been reported. Very recently similar methods were applied to the study of Rh monoatomic rows on the Ag(001) surface.[13] From the experimental point of view, only modern techniques like scanning tunneling microscopy (STM) (Refs. 14–16) and molecular beam epitaxy (MBE) together with real-time control of the deposition stage obtained by thermal energy atom scattering (TEAS) (Refs. 17–19) provided recently the tools for the realization of such one-dimensional (or quasi-one-dimensional) systems. The particular morphology of the fcc (110) surface, composed of close-packed rows of atoms separated by channels, was used as a template to grow linear Cu chains[16,20] by diffusion-controlled aggregation at Pd(110) surfaces. Even more suited to growing one-dimensional structures have proved to be the vicinal surfaces (or high-Miller-index surfaces) which, with their ordered array of steps, present an ideal template for the growth of wire superlattices by means of step decoration. Persuing this idea the Kern group in Lausanne succeeded in the growth of monoatomic metal chains on Pt(997) (Refs. 18,21 and 19); this system has been also recently studied by a kinetic Monte Carlo model.[22] In previous experimental attempts only multiatomic rows were obtained[23,24] with widths of the order of a few nanometers.

Similarly to the experimental methods, we here exploit the concept of step decoration of vicinal surfaces and present calculations from first principles for the magnetic moments of 4*d* monoatomic rows on fcc Ag vicinal substrates. This work was motivated by previous results obtained in our group for finite-size 4*d* magnetic nanostructures (finite-length chains and islands) adsorbed on the Ag(001) surface.[25] The present results for the monoatomic rows (one dimension) can be viewed as the completion of the study of low-dimensional 4*d* structures on the Ag(100) surface, together with the results existent in the literature for single 4*d* adatoms (zero dimension) (Ref. 5) and monolayers (two-dimensions) (Ref. 2).

This paper is organized as follows: In Sec. II we describe briefly the method of calculation together with the systems investigated. In Sec. III we discuss the ferromagnetic solutions for the 4*d* monoatomic rows on different Ag vicinal

surfaces, and we investigate the trend for ferromagnetic and antiferromagnetic coupling between the row atoms for the fcc (711) Ag vicinal substrate. In Sec. IV we summarize the obtained results.

II. METHOD OF CALCULATION

A. Computational approach

The calculations are based on density functional theory (DFT) in the local density approximation (LDA) and a recently implemented version of our screened Korringa-Kohn-Rostoker (KKR) Green's function method[26–28] enable one to treat systems with an arbitrary number of atoms in the unit cell and arbitrary two-dimensional or three-dimensional cell periodicity. A repulsive muffin-tin potential (4 Ry high) is used as a reference system, transforming the usual ''free-space'' long-ranged structure constants into exponentially decaying ones. For layered systems the advantage of this transformation is the *N*-scaling behavior (*N* the number of layers in the system) and the corresponding reduction of computer time in the solution of the Dyson equation, allowing us to treat much bigger systems compared to the traditional KKR Green's function method. The potentials were assumed to be spherically symmetric inside the Wigner-Seitz sphere as in the atomic sphere approximation (ASA) but a multipole expansion of the charge density has been taken into account up to $l_{MAX}=6$ (angular momenta up to $l_{MAX}=3$ have been used for the wave functions). For the exchange correlation functionals the expression given by Vosko, Wilk and Nusair[29] fitted to Monte Carlo results for the homogeneous electron gas (jellium) (Ref. 30) has been used. Energy integrations were performed along a contour which extends from the bottom of the valence band into the complex plane[31] and returns to the real-energy axis at the Fermi energy. Due to the smooth behavior of the Green's function for complex energies, only few energy points, i.e., ~ 25, have been necessary. Brillouin zone (BZ) samplings have been performed by means of special points methods.[32] For the high-Miller-index surface under interest, typically few tens of $\mathbf{q}_{||}$ points are needed to sample the irreducible parts of the two-dimensional BZ for complex energies far away from the real axis, while up to 300 $\mathbf{q}_{||}$ points were necessary close the real axis near the Fermi level.

B. Step edges and vicinal surfaces

In order to simulate the monoatomic rows, we used the concept of a *vicinal surface*. When we cut the crystal with a plane perpendicular to a high-Miller-index direction (vicinal surface) we obtain a superlattice of regularly separated steps of monoatomic height; all the step edges (the ones with kinks as well) can be obtained by a particular set of Miller indices (for a systematic study of the vicinal surfaces for an fcc crystal we refer to the work of Van Hove and Somorjai.[33]) On each side of an fcc Ag slab tilted by the proper Miller indices we placed one high-index 4*d* overlayer which is composed of an array of monoatomic rows separated by low-Miller-index terraces, the width of which depends on the particular orientation of the vicinal substrate. Moreover, simply inserting some ''vacuum'' layers between the 4*d* vicinal overlayers and the Ag substrate, we can actually move the rows from the step edge towards the middle of the terraces. Due to the long range of the magnetic interactions, the monoatomic rows interact slightly with each other through the Ag substrate. Because of that, small changes in the moments and in the stability of the magnetic solutions are expected with respect to the case of isolated monoatomic rows. One can avoid such row-row interactions by considering a sufficiently thick Ag substrate with sufficiently wide terraces. On the other hand, the wider the terraces, the smaller the interlayer distance between the vicinal layers; consequently, the number of vicinal layers which has to be taken into account for a certain substrate thickness increases as well.

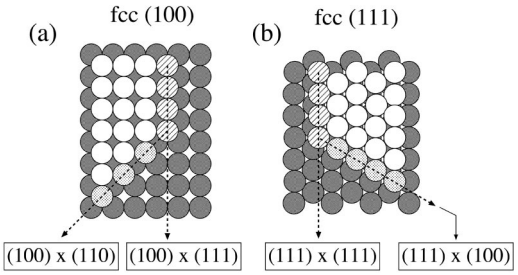

FIG. 1. Step edges at the (a) fcc (100) and (b) fcc (111) terraces; the ''step notation'' from Ref. 33 is used.

We depict in Figs. 1(a) and 1(b) step edges on the fcc (100) and (111) terraces. On the fcc (100) terrace two different step edges are most important; we indicate them, following the ''step notation'' introduced by Van Hove and Somorjai,[33] as $(100)\times(111)$ and $(100)\times(110)$. The $(100)\times(111)$ step is close packed; i.e., the atoms along the step edge in the $\langle 110\rangle$ direction are nearest neighbors (NN), with $\{111\}$ faceting and coordination number $N_c=7$, while the $(100)\times(110)$ is an open step; i.e., the step atoms are next nearest neighbors (NNN) along the $\langle 100\rangle$ direction, with $\{110\}$ faceting and coordination number $N_c=6$. Also for the fcc (111) terrace two different steps are shown, the $(111)\times(111)$ and $(111)\times(100)$. Both step edges are close packed along $\langle 110\rangle$ directions and have coordination number $N_c=7$, differing only in the orientation of the microfacets, i.e., $\{111\}$ and $\{100\}$.

Since in the following we will mainly concentrate on the step edges on the (100) terrace, we describe in more detail the surfaces vicinal to the (100) surface. The two families of high-Miller-index surfaces which cut the crystal along the $(100)\times(111)$ and $(100)\times(110)$ step edges have, respectively, Miller indices $(2m-1,1,1)$ and $(m,1,0)$; the terraces exhibited by these vicinal surfaces are, respectively, m and $(m+1)$ atomic rows wide. We have chosen the fcc (711) (see Fig. 2) and fcc (410) (see Fig. 3) vicinal surfaces which exhibit terraces being four atomic rows wide. In order to obtain a good ''bulk'' description of the inner part of the Ag slabs, simultaneously decoupling the two row arrays on the two sides of the Ag slabs, we considered a thickness of 14 and 18 Ag layers in the tilted direction, respectively, for the fcc (711) and fcc (410) orientations (while the substrates depicted in Figs. 2 and 3 contain both 14 Ag layers). Some

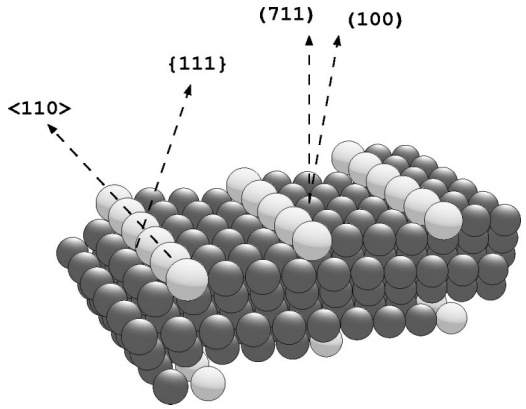

FIG. 2. The fcc (711) vicinal substrate considered to characterize the monoatomic rows at the (100)×(111) step edge.

''vacuum'' vicinal layers, i.e., six, are then placed at both sides of the slabs. Test calculations have shown that the magnetic moments of the monoatomic 4*d* rows changed by no more than few hundredths of μ_B, when up to four Ag vicinal layers were added in the substrates, showing that the rows are sufficiently well decoupled.

III. RESULTS AND DISCUSSION

In the following we present calculations for the magnetic moments of monoatomic 4*d* rows at different step edges and terrace positions of Ag vicinal surfaces. It is well known that the elements at the beginning and in the middle of the transition metal series (3*d*, 4*d*, and 5*d*) often prefer configurations with antiferromagnetic (AFM) coupling.[34] Since the study of AFM solutions for the monoatomic rows requires a much larger computational effort, we investigated AFM coupling between the atom in each row only for the monoatomic rows at the (100)×(111) step edge and discuss them separately in Sec. III B.

A. Ferromagnetic solutions

The results for 4*d* magnetic monoatomic rows on fcc (711) and fcc (410) Ag vicinal surfaces are shown in Fig. 4. For both step orientations the rows were placed directly at step edges or in the middle of the terraces; the latter geometry allows us to compare with the results for finite-length chains on the Ag(100) surface which were obtained previously.[25] For the sake of simplicity we will refer from now on to the different rows by using the ''step notation'' introduced above.

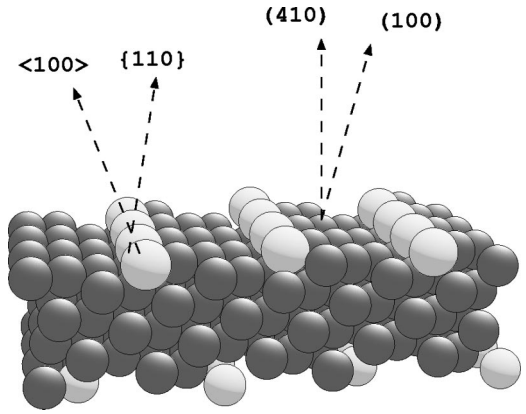

FIG. 3. The fcc (410) vicinal substrate considered to characterize the monoatomic rows at the (100)×(110) step edge.

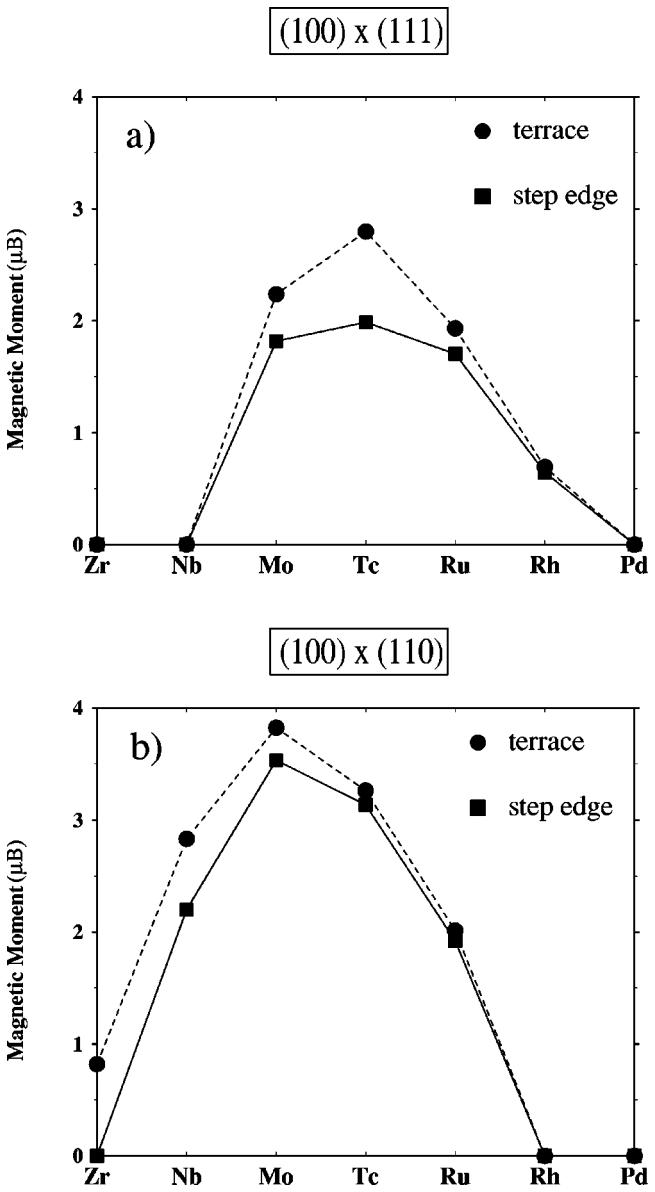

FIG. 4. Magnetic moments of 4*d* monoatomic rows (a) on the fcc Ag(711) and (b) on the fcc Ag(410) vicinal surfaces, used to simulate, respectively, the close-packed (100)×(111) and open (100)×(110) rows. The rows were placed both in terrace (circles) and step edge (squares) positions of the (100) Ag terraces.

A direct comparison between the magnetic moment profiles for the two different step orientations shows that the magnetic moments for the (100)×(111) rows are smaller than the ones for the (100)×(110) rows for all the elements except Rh. The main reason for this decrease in the magnetic moments is the 4*d*-4*d* hybridization acting between the atoms in each row which is much larger for the close-packed rows than for the open rows, where neighboring row atoms

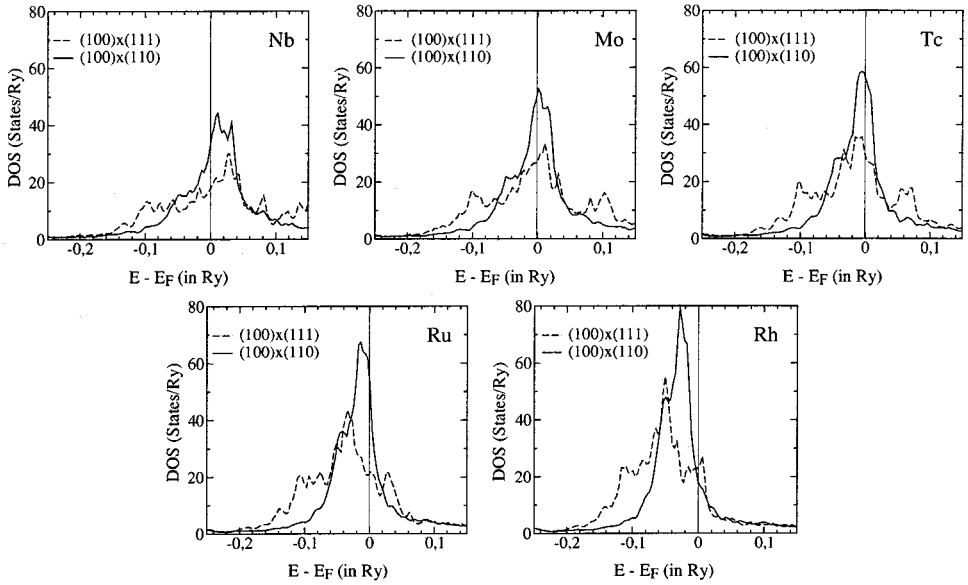

FIG. 5. Paramagnetic density of states (DOS) for the 4*d* elements from Nb to Rh at the close-packed $(100)\times(111)$ and open $(100)\times(110)$ step edges.

are separated by a second-neighbor distance. The role of the 4*d* hybridization was already discussed by Blügel[2] in the case of 4*d* monolayers on Ag, Au, and Pd (001) surfaces and by Willenborg *et al.*[35] in the case of single impurities and dimers in bulk Ag. The *d*-*d* hybridization between the 4*d* orbitals increases the bandwidth of the *d* states, thus broadening the density of states (DOS) $n(E)$ obtained, e.g., in a paramagnetic calculation. This broadening has two different effects depending on the position of the virtual bound-state peak relatively to the Fermi energy E_F; if the peak is very near to the Fermi energy, a broadening in the bands causes a reduction of the DOS at the Fermi level (e.g., the Mo case), while if the peak is below E_F, it can produce the opposite effect and the DOS increases at E_F (e.g., in the Rh case).

We illustrate this behavior in Fig. 5 showing the DOS in a non-spin-polarized calculation for the elements from Nb to Rh in the 4*d* series at the close-packed $(100)\times(111)$ and open $(100)\times(110)$ step edges. Since in the open rows the interatomic distance is the one of second-neighbor bulk atoms, the hybridization between the 4*d* orbitals is sufficiently weak and the atoms in the row behave, regarding their magnetic properties, practically like isolated adatoms. Indeed the calculated local moments for these rows are very similar to the results obtained in Ref. 25 for the single adatoms. Therefore the DOS for these rows shown in Fig. 5 by the solid lines resembles well the Lorentzian DOS of single adatoms and is considerably narrower than the DOS of the close-packed rows (dashed lines in Fig. 5). Within the Stoner model, the criterium $n(E_F)I>1$ (with the exchange integral I) presents a necessary condition for the existence of a ferromagnetic solution. Thus a high DOS at the Fermi level favors a local moment. To get an estimate for I, we consider the critical case of Rh rows, being paramagnetic for the open configuration [Fig. 4(b)]. From the Rh DOS in Fig. 5, we estimate in this way a critical DOS value at E_F of 20 states/Ry, yielding an exchange integral $I=0.05$ Ry, being consistent with the value computed by Janak.[36] Assuming the same exchange integral also for the other 4*d* elements we conclude that 20 states/Ry is the critical threshold value for the existence of a ferromagnetic solution. As shown in Fig. 5, the DOS at the Fermi energy for Mo, Tc, and Ru exceeds this offset value for both the step edges, correctly predicting ferromagnetic solutions in all cases. At the beginning of the 4*d* series, the Stoner criterium is also able to describe the more critical case of Nb, which presents a ferromagnetic solution only at the open step edge.

Resuming, the increase of the hybridization between the atoms in each row reduces the magnetic moments for all the elements up to Ru since the virtual bound-state peak is sufficiently close to the Fermi energy, while it enhances the magnetic moment for Rh. As observed by Blügel[2] the reduction of the magnetic moments from the single adatoms to the monolayer is accompanied with a progressive shift of the maximum to higher valences; this is also observed in our case when one compares the results for the open rows with the close-packed ones for which the maximum shifts from Mo to Tc (see Fig. 4). The strong 4*d*-4*d* hybridization present between the nearest-neighbor atoms at the close-packed $(100)\times(111)$ rows quenches the moments of Zr and Nb and reduces the magnetic moment of Mo up to more than 40%. This reduction become less and less efficient, moving to the end of the series, and for Rh the opposite trend is observed and a small moment of around $0.6\mu_B$ is predicted for the close-packed row.

The present results for the 4*d* rows can be viewed as the one-dimensional link between the zero-dimensional systems represented by the single adatoms and the two-dimensional systems represented by the monolayers. We can thus summarize in Fig. 6 the results for these three different systems being adsorbed on the Ag(001) surface, by including the results for the adatoms obtained by Lang *et al.*[5] and the results for the monolayers obtained by Blügel[2]; for the rows the results for the close-packed direction are given in Fig. 6. With increasing dimensions the increase in the 4*d*-4*d* hybridization leads to the progressive decrease of the local moments for the elements at the beginning and center of the

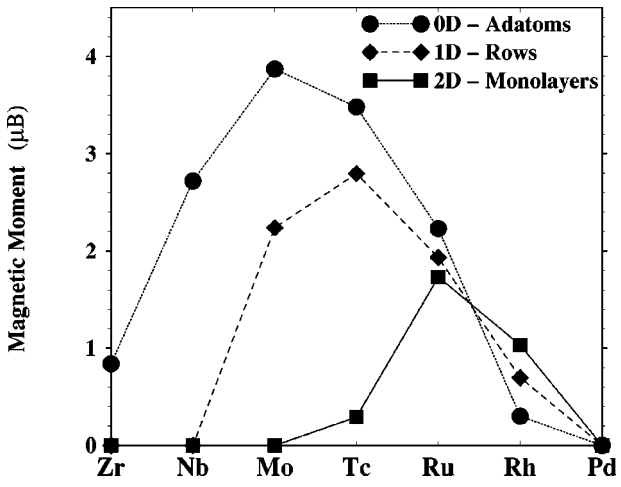

FIG. 6. Effect of the dimensionality on the magnetic moment profile. Shown are the results for adatoms (circles) (Ref. 5), infinite close-packed rows (diamonds), and monolayers (squares) (Ref. 2) of the 4*d* elements on the Ag(001) surface.

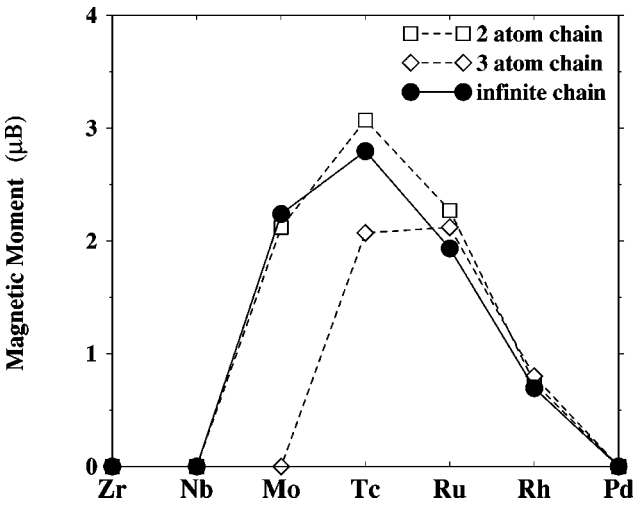

FIG. 7. Comparison between the magnetic moments of finite-length 4*d* chains (Ref. 25) and infinite ones [for close-packed rows, Fig. 4(a), solid circles] on the Ag(001) surface.

series and to a simultaneous shift of the maximum in the moment profile towards higher valences which is assumed, respectively, by Mo for the adatoms, by Tc for the adsorbate rows, and by Ru for the overlayers. In the limit of three-dimensional systems, i.e., bulk crystals, this reduction is strong enough to quench the magnetic moments of all the elements and no ferromagnetism is observed for the whole 4*d* series.

Another evident feature from Figs. 4(a) and 4(b) is that when the magnetic rows are shifted from the middle of the terraces (dashed lines) to the step edges (solid lines), for both the orientations, a decrease of the magnetic moments is observed. This is due to the increase in the hybridization between the extended 4*d* wave functions of the row atoms and the *sp*-like valence electrons of the Ag step atoms. This mechanism was also observed when free 4*d* dimers were compared with dimers adsorbated on the Ag(001) surface;[25] in that case, the hybridization with the Ag substrate was rather important so that magnetism was completely quenched for the free dimers in the beginning of the 4*d* series (Y,Zr,Nb), while the magnetic moment of Mo was reduced by a factor of 2. Since the magnetic moments are only sensitive to the local environment and in a good approximation only to the first atomic shell, i.e., to the coordination number N_c, the decrease in the magnetic moments can be described by an increase in N_c for the row atoms from the terrace position to the step edge position. As can be easily deduced from Fig. 1, moving from the terrace to the step edge a row atom gains, respectively, two Ag neighbors for the open $(100)\times(110)$ row and only one Ag neighbor for the close-packed $(100)\times(111)$ row. Another general feature is that the reduction of the magnetic moments is more enhanced in the beginning of the 4*d* series. This has its justification in the larger spatial extent of the 4*d* orbitals for the elements with lower valences in the series; in short, the earlier elements are more sensitive to the environmental changes than the elements at the end of the series.

We can now proceed comparing the present results for the infinite rows with the results obtained by Wildberger *et al.*[25] for small 4*d* chains on the Ag(001) surface, which initiated the present study. In that work, an unusual oscillatory behavior was predicted for the magnetic moments of finite-length 4*d* chains as a function of the chain length; only chains along the $\langle 110\rangle$ direction, i.e., the close-packed one, were investigated and only up to four atom chains were studied. The results for the 4*d* close-packed rows at the terrace position [open circles in Fig. 4(b)] may thus be viewed as an extension to an infinite length of chains presented by Wildberger *et al.*[25] Their prediction of the existence of finite moments in the limit of infinite chains is thus verified by the present results. In order to compare quantitatively the magnetic moments, we include in Fig. 7 the results for the infinite rows together with the magnetic moments for the two-atom and three-atom chains; the magnetic moments presented for the finite-length chains are in reality an ''average,'' since atoms along the chain have different moments depending on the position in the chain (i.e., in the middle or at the end). We do not include the results for the four-atom chain since their magnetic moments are almost equivalent to the ones of the dimers (see Fig. 3 in Ref. 25). It is evident from Fig. 7 that the magnetic moments for the infinite rows resemble very well the ones for the dimers and the four atom chains, and differ sensibly from the trimers for Mo and Tc. Since no results are available for longer chains, it is difficult to say whether a true oscillatory behavior for the magnetic moments exists as a function of the chain length or if the results for the trimers have to be considered as an ''exception.'' The close agreement between the infinite rows and the four-atom chains suggests that the latter interpretation is more probable and that eventually only minor oscillations are expected to appear for longer chains of atoms. The only work, to our knowledge, which discuss the magnetic behavior for finite-length N-atom chains, with $N>4$, was performed by Dorantes-Dávila and Pastor,[11] who studied the MAE for Fe and Co chains by means of a tight-binding Hamiltonian.

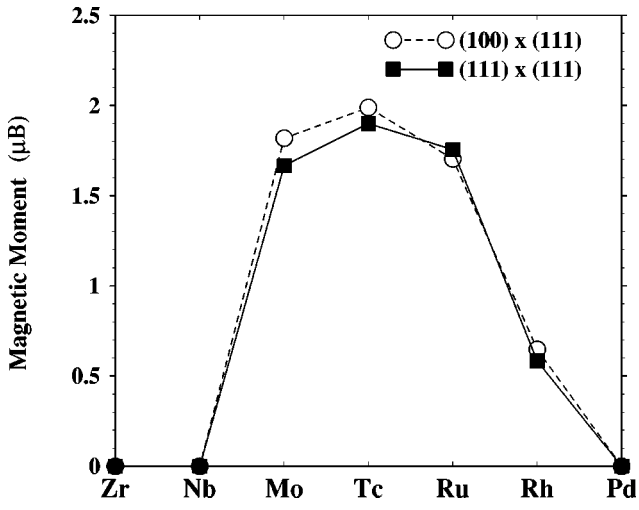

FIG. 8. Comparison between the magnetic moment profile of the 4*d* rows on the (100)×(111) and (111)×(111) step edges; both step edges show close packing in the row direction and the same coordination number $N_c=7$.

To summarize, the magnetic moments of the 4*d* monoatomic rows at different step edges is driven mainly by two mechanisms, i.e., the 4*d*-4*d* hybridization acting between the atoms in each row and the 4*d*-*sp*-like hybridization between the row atoms and the Ag substrate atoms, the first hybridization mechanism being controlled by the interatomic distance in the row and the second by the coordination number and the faceting of the row atoms. As shown in Fig. 1(b) the fcc (111) terraces offer two step edges, both close packed and both with coordination number $N_c=7$, the (111)×(111) and the (111)×(100). From the above discussion, they should both induce similar magnetic properties as the (100)×(111) step edge which is also close packed and has the same coordination number $N_c=7$. In the following we present a comparison between the magnetic moment profiles of the 4*d* rows at the (100)×(111) and at the (111)×(111) step edges. The class of vicinal surfaces that cut the fcc crystal along the (111)×(111) step edge has Miller indices $(m,m,m-2)$, which has *m* rows in the terraces. Since terraces composed of four atomic rows are sufficiently wide in order to neglect the step-step interactions, we have chosen the fcc (221) Ag vicinal surface [which is the (442) in the above notation, but it is common to remove a constant multiplicative factor from the Miller indices].

As shown in Fig. 8, the magnetic profiles obtained placing the 4*d* rows on the two step edges, i.e., (100)×(111) and the (111)×(111), are indeed very similar. The only difference in the local environment for an atom sitting at the two step edges is that the NN are distributed differently in the upper and lower terraces. More precisely for the (100)×(111), four NN are on the lower terrace and three on the upper terrace (with two of these three in the row direction), while for the (100)×(111) step edge three NN are in the lower terrace and four in the upper one (with two of these four in the row direction). This small difference induces for Mo and Tc a difference of around $0.2\mu_B$ and for the other 4*d* elements a difference of less than $0.1\mu_B$ in the magnetic moments. This finding completely supports the above description of the dependence of the magnetic moments on the local environment, i.e., the coordination number and the packing of the atoms in the rows.

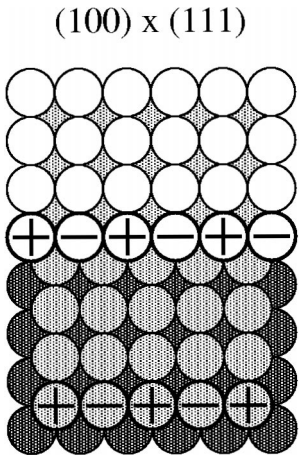

FIG. 9. Antiferromagnetic coupling in the rows at the (100)×(111) step edge; the + 's and − 's indicate the different alignments of the magnetic moments.

B. Antiferromagnetic solutions

Up to now we discussed only the ferromagnetic solutions found for the 4*d* monoatomic rows on the Ag substrates. But it is well known from general theorems about tight-binding bands[34] that there is a tendency towards antiferromagnetism for elements in the middle of transition metal series. Indeed antiferromagnetic solutions were obtained for finite-length 4*d* chains[37,38] and by means of total energy calculations they were predicted to be the more stable solutions for Nb and Mo dimers on the Ag(100) terrace.

In the case of antiferromagnetic ordering between the atoms in each row it is necessary to double the periodicity along the row direction, i.e., double the number of inequivalent atoms in the systems. Because of the increase in the computational effort, we investigated the antiferromagnetic solutions only for the (100)×(111) 4*d* rows, simulated by the fcc (711) Ag vicinal surface; the antiferromagnetic order in the rows at this step edge is depicted in Fig. 9. The slabs considered for these calculations contain 60 inequivalent atoms, i.e., 30 layers and 2 inequivalent atoms per layers; 18 Ag layers in the substrate were considered and embedded between 5 vacuum layers on each side. Because of the extreme computational demand of the present calculations, a parallelized version of the SKKR code turned out to be very helpful, relieving sensibly the time needed to converge the systems.

In Table I, we list the results for the magnetic moments for both ferromagnetic (FM) and antiferromagnetic solutions, together with the differences in the total energies between the FM or AFM solutions and the paramagnetic (P) ones, i.e., $\Delta E^{FM}=E^P-E^{FM}$ and $\Delta E^{AFM}=E^P-E^{AFM}$; the paramagnetic solutions were obtained by means of non-spin-polarized calculations. AFM solutions with large magnetic moments were found for Mo, $m_{AFM}=\pm 2.72\ \mu_B$, and Tc,

TABLE I. Ferromagnetic (FM) vs antiferromagnetic (AFM) solutions for the 4*d* monoatomic rows at the (100)×(111) step edge; in the upper table (a) the magnetic moments for the FM and AFM case and in the lower table (b) the total energies for the FM and AFM solutions relative to constrained paramagnetic (P) calculations are listed, i.e., $\Delta E^{FM}=E^{P}-E^{FM}$ and $\Delta E^{AFM}=E^{P}-E^{AFM}$. The most stable configurations have the higher-energy difference and are indicated by bold numbers.

(a)

Magnetic moments (μ_B)	Nb	Mo	Tc	Ru	Rh
Ferro	–	1.85	**1.92**	**1.65**	**0.59**
Antiferro	±**0.83**	±**2.72**	±2.06	–	–

(b)

Total energy (mRy)	Nb	Mo	Tc	Ru	Rh
ΔE^{FM}	–	+10.2	**+15.7**	**+7.3**	**+1.5**
ΔE^{AFM}	**+0.7**	**+18.8**	+14.3	–	–

$m_{AFM}=\pm 2.06\ \mu_B$, while a smaller magnetic moment has been found for Nb, $m_{AFM}=\pm 0.83\ \mu_B$.

From total energy calculations, as shown in Table I, the Mo row is predicted to be more stable in the AFM configuration than in the FM one, while for Tc the two solutions (FM and AFM) are almost degenerate in energy. Nb shows no FM solutions while in the AFM case a magnetic moment of $\pm 0.83\mu_B$ is found. Ru and Rh show only FM solutions. These results are in good agreement with the calculations performed for the 4*d* dimers on the Ag(001) surface.[38] In the case of the 4*d* dimers the energy difference between the AFM and the FM solutions is systematically larger than the difference $\Delta E=\Delta E^{FM}-\Delta E^{AFM}$ in Table I. For example, for a Mo dimer the AFM state is more stable than the FM one, with moments, respectively, of $m_{AFM}=3.17\mu_B$ and $m_{FM}=2.12\mu_B$,[37] and an energy difference of about 50 mRy.[38] For the Mo row a much smaller energy difference ΔE between FM and AFM solutions is obtained, i.e., $\Delta E=8.6$ mRy. The 4*d* monolayers with FM ordering on the Ag(001) surface[2] showed total energies with similar order of magnitude; the largest magnetic moment was found for Ru, $m=1.73\mu_B$ with $\Delta E_{FM}=6.7$ mRy above the paramagnetic solutions. From the above picture it is therefore evident that, for the 4*d* series, moving from the lower coordinated systems (dimers) to the more coordinated ones (rows and monolayers) the magnetic solutions become progressively less stable in comparison to the paramagnetic ones. In the limit of maximum possible coordination, i.e., as bulk materials, indeed all the elements in the 4*d* series are predicted to be nonmagnetic.

Finally we have to point out that in the present calculations the atoms were fixed in their ideal positions; i.e., no atomic relaxations are included in the calculations. The relaxations at the step edges usually try to smooth the step edges; i.e., inward relaxation towards the substrate is expected for the step atoms. The size of the total energy differences ΔE^{FM} and ΔE^{AFM} can be viewed as an indication of the stability of the magnetic solutions with respect to such environmental changes. Looking at the values in Table I we see, for instance, that the FM configuration of Rh and the AFM configuration of Nb are only marginally more stable than the paramagnetic ones and might thus be affected by relaxation effects.

IV. SUMMARY

We presented *ab initio* results for the magnetic properties of 4*d* monoatomic rows on different Ag vicinal substrates. We exploited, similar to the experiments, the concept of a vicinal (or high-Miller-index) surface to characterize an ordered array of monoatomic rows. The magnetization profile of the 4*d* rows has been investigated, placing the rows at terrace and step edge positions of three different high-Miller-index surfaces, i.e., (711), (410), and (221), of fcc Ag. The results can be explained by the coordination number of the row atoms and by the hybridization acting between the extended 4*d* orbitals of the row atoms and the *sp* valence electrons of the Ag substrate atoms. The effect of the dimensionality on the magnetic properties was also discussed, comparing the results for the monoatomic rows with the ones in the literature for 4*d* adatoms, finite-length chains, and monolayers on the Ag(001) surface. The results obtained in this work for the monoatomic rows are in complete agreement with the picture proposed in the literature for adatoms, finite-length chains, and monolayers, showing how the increase in the hybridization between the 4*d* atoms leads to the progressive decrease of the local moments for the elements at the beginning and center of the series and to a simultaneous shift of the maximum in the moment profile towards higher valences. For the fcc (711) Ag substrate we investigated the occurrence of antiferromagnetic coupling between the atoms in each row and discussed the stability of the AFM solution with respect to the FM ones. In detail, we found that Nb exhibits only the AFM solution while only two elements present both FM and AFM solutions, i.e., Mo and Tc; while the AFM solution of Mo is clearly the most stable one, the FM and AFM solutions for Tc are almost degenerate in energy.

[1] F. J. Himpsel, J. E. Ortega, G. J. Mankey, and R. F. Willis, Adv. Phys. **47**, 511 (1998).
[2] S. Blügel, Europhys. Lett. **18**, 257 (1992).
[3] S. Blügel, Phys. Rev. Lett. **68**, 851 (1992).
[4] R. Wu and A. J. Freeman, Phys. Rev. B **45**, 7222 (1992).
[5] P. Lang, V. S. Stepanyuk, K. Wildberger, R. Zeller, and P. H. Dederichs, Solid State Commun. **92**, 755 (1994).
[6] V. S. Stepanyuk, W. Hergert, K. Wildberger, R. Zeller, and P. H. Dederichs, Phys. Rev. B **53**, 2121 (1996).
[7] R. Podloucky, R. Zeller, and P. H. Dederichs, Phys. Rev. B **22**,

5777 (1980).
[8] R. Schäfer and G. Bergmann, Solid State Commun. **98**, 45 (1996).
[9] H. Beckmann, R. Schäfer, W. Li, and G. Bergmann, Europhys. Lett. **33**, 563 (1996).
[10] H. Beckmann and G. Bergmann, Phys. Rev. B **55**, 14 350 (1997).
[11] J. Dorantes-Dávila and G. M. Pastor, Phys. Rev. Lett. **81**, 208 (1998).
[12] R. Robles, J. Izquierdo, and A. Vega, Phys. Rev. B **61**, 6848 (2000).
[13] D. I. Bazhanov, W. Hergert, V. S. Stepanyuk, A. A. Katsnelson, P. Rennert, K. Kokko, and C. Demangeat, Phys. Rev. B **62**, R6415 (2000).
[14] M. F. Crommie, C. P. Lutz, and D. M. Eigler, Science **262**, 218 (1993).
[15] F. Besenbacher, Rep. Prog. Phys. **59**, 1737 (1996).
[16] H. Röder, E. Hahn, H. Brune, J.-P. Bucher, and K. Kern, Nature (London) **366**, 141 (1993).
[17] M. Blanc, K. Kuhnke, V. Marsico, and K. Kern, Surf. Sci. **414**, L964 (1998).
[18] P. Gambardella, M. Blanc, H. Brune, K. Kuhnke, and K. Kern, Phys. Rev. B **61**, 2254 (2000).
[19] A. Dallmeyer, C. Carbone, W. Eberhardt, C. Pampuch, O. Rader, W. Gudat, P. Gambardella, and K. Kern, Phys. Rev. B **61**, R5133 (2000).
[20] J.-P. Bucher, E. Hahn, P. Fernandez, C. Massobrio, and K. Kern, Europhys. Lett. **27**, 473 (1994).
[21] P. Gambardella, M. Blanc, L. Bürgi, K. Kuhnke, and K. Kern, Surf. Sci. **449**, 93 (2000).
[22] F. Picaud, C. Ramseyer, C. Girardet, and P. Jensen, Phys. Rev. B **61**, 16 154 (2000).
[23] O. Fruchart, M. Klaua, J. Barthel, and J. Kirschner, Phys. Rev. Lett. **83**, 2769 (1999).
[24] J. Shen, R. Skomski, M. Klaua, H. Jenniches, S. S. Manoharan, and J. Kirschner, Phys. Rev. B **56**, 2340 (1997).
[25] K. Wildberger, V. S. Stepanyuk, P. Lang, R. Zeller, and P. H. Dederichs, Phys. Rev. Lett. **75**, 509 (1995).
[26] R. Zeller, P. H. Dederichs, B. Újfalussy, L. Szunyogh, and P. Weinberger, Phys. Rev. B **52**, 8807 (1995).
[27] R. Zeller, Phys. Rev. B **55**, 9400 (1997).
[28] K. Wildberger, R. Zeller, and P. H. Dederichs, Phys. Rev. B **55**, 10 074 (1997).
[29] S. H. Vosko, L. Wilk, and N. Nusair, Can. J. Phys. **58**, 1200 (1980).
[30] D. M. Ceperley and B. J. Alder, Phys. Rev. Lett. **45**, 566 (1980).
[31] R. Zeller, J. Deutz, and P. H. Dederichs, Solid State Commun. **44**, 993 (1982).
[32] H. J. Monkhorst and J. D. Pack, Phys. Rev. B **13**, 5188 (1976).
[33] M. A. Van Hove and G. A. Somorjai, Surf. Sci. **92**, 489 (1980).
[34] V. Heine and J. H. Samson, J. Phys. F **13**, 2155 (1983).
[35] K. Willenborg, R. Zeller, and P. H. Dederichs, Europhys. Lett. **18**, 263 (1992).
[36] J. F. Janak, Phys. Rev. B **16**, 255 (1977).
[37] K. Wildberger, Ph.D. thesis, RWTH-Aachen, 1994.
[38] V. S. Stepanyuk, W. Hergert, P. Rennert, K. Wildberger, R. Zeller, and P. H. Dederichs, Phys. Rev. B **54**, 14 121 (1996).